NANOSYSTEMS: PHYSICS, CHEMISTRY, MATHEMATICS, 2017, 8 (5), P. 620–627

Redistribution of Mg and Ni cations in crystal lattice of conical nanotube with chrysotile structure

A. A. Krasilin, V. V. Gusarov

Ioffe Institute, Politekhnicheskaya st., 26, St. Petersburg, 194021, Russia

ikrasilin@mail.ioffe.ru

PACS 64.70.Nd **DOI 10.17586/2220-8054-2017-8-5-620-627**

Recently, nanotubular hydrosilicates have attracted attention due to numerous possible applications and intriguing formation mechanism. In this study we estimate energy effect of cylindrical and conical $(Mg_{0.5},Ni_{0.5})_3Si_2O_5(OH)_4$ nanotube formation depending on their size parameters, cone angle, and Mg–Ni redistribution function. The calculations show that, as we expected, conical morphology is less preferable from an energy perspective than the cylindrical one, and the energy difference between them increases with the cone angle. Nevertheless, Mg and Ni cations redistribution along side length decreases strain energy of conical nanotube. This effect reaches its maximum of ~ -75 kJ/mol at a cone angle of 5°.

Keywords: hydrosilicate, chrysotile, nanotube, nanoscroll, hydrothermal synthesis, modeling, morphology.

Received: 30 August 2017

Revised: 2 September 2017

1. Introduction

The unusual behavior and properties of substances in nanotubes and related composite materials have resulted in wide scientific and technological interest [1–5]. In addition to well-known carbon [6], nitride [7], and chalcogenide nanotubes [8], researchers, using different approaches, have obtained new representative structures, termed micro- and nanoscrolls [9–16].

In the last few decades, spontaneously scrolling nanotubular hydrosilicates like imogolite, halloysite, and chrysotile have garnered increased attention due to their application as polymer fillers [17–19] (i.e. an alternative to carbon and chalcogenide nanotubes [20, 21]), sorbents and drug containers [22–24], catalyst materials [25–28], and materials for Li-ion energy sources [29]. The high specific surface (up to several hundred m^2/g [30–32]), abundance of OH-groups, and synthetic flexibility made hydrosilicate nanotubes and nanoscrolls suitable for these purposes. In addition, wide array of constituents (Mg, Al, Si) grants possibility of large-scale production and even industrial mining. The study of phase composition for hydrosilicate systems is of high importance for understanding of a number of geological processes [33, 34]. The potential of self-scrolling lies in one crystal structure peculiarity (Fig. 1, chrysotile structure as an example): one hydrosilicate layer consists of two sublayers (MgO_6 octahedra and SiO_4 tetrahedra) with slightly different lattice parameters. Covalent bonding of the sublayers causes internal stress in the layer, and nanotube formation is one effective relaxation mechanisms.

The bending, scrolling of crystal layer, and formation of chrysotile (and related minerals) nanotubes itself is of substantial interest. Since the middle of 20th century, various research groups have focused on synthesis of pure Mg-chrysotile [38–41], and related Fe [42, 43], Co [44], Ni-doped [45–49] structural analogs. The principal goal of recent studies in this field was to reveal pre-nucleus states that take part in the nanotube formation, and determine the role of their structure in the nanotube formation process. Other researches have opted to take theoretical consideration of the problem and performed hydrosilicate structure modeling [50–52] which yielded information about the preferred radius of curvature, electronic, and mechanical properties of those materials. Another theoretical approach involves phenomenological energy modeling [53–58], which focuses more on the morphological issues of single- and multiwalled nanotubes. In particular, it helps not only to predict preferable multiwalled nanotube size parameters, but to understand in deep the nanotubes' size distributions observed in electron microscopy experiments [59].

Varying the chemical composition affects morphology and properties of hydrosilicate nanotubes. Depending on its nature, the guest cation can increase the nanotube diameter, transform nanotubes into plates [43, 60–63], and provoke the formation of second nonsilicate phases. Apparently, the general trend for any cation doping of hydrosilicate nanotubes is formation of nanotubes and nanoscrolls with morphologies that deviate from cylinders. The SEM-image on Fig. 1 demonstrates particular example of this deviation: formation of conical $(Mg_{0.5},Ni_{0.5})_3Si_2O_5(OH)_4$

nanoscrolls. Usually, the formation of conical nanotubes and nanoscrolls depends mainly on the pH of the hydrothermal medium [64]. Recently, we revealed [35] that partial Mg^{2+} to Ni^{2+} substitution yields a 3–5 fold increase of conical nanoscrolls content obtained in water and aqueous NaOH solutions. We try to investigate here possible mechanisms that stand behind this effect by further development of the energy approach proposed in [57, 59].

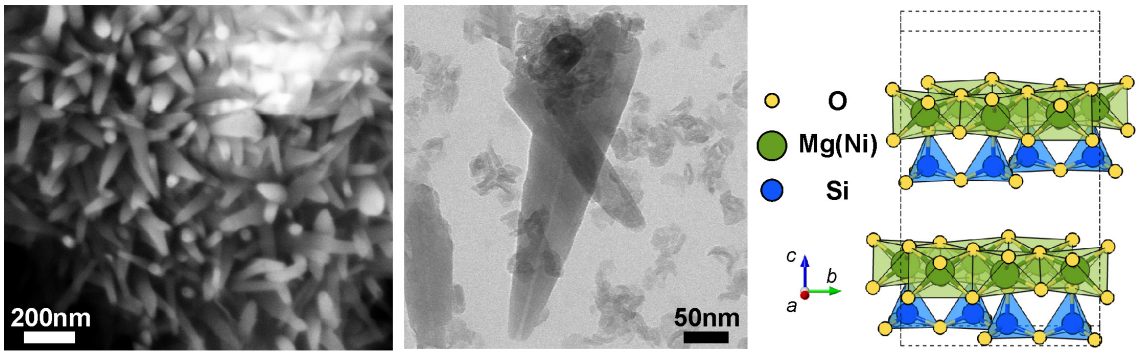

FIG. 1. SEM and TEM images of conical $(Mg_{0.5},Ni_{0.5})_3Si_2O_5(OH)_4$ nanoscrolls with chrysotile structure, obtained under hydrothermal conditions [35], and chrysotile unit cell (visualized using VESTA software [36]) according to data in [37]. Layers are joined by hydrogen bonds (not shown)

2. Energy model

The energy model proposed here relies on equations for the case of singlewalled hydrosilicate nanotube formation that were previously obtained in [57]. We compare four different states of hydrosilicate bilayer with chrysotile structure (Fig. 2): flat layer, cylindrical singlewalled nanotube, conical nanotube with uniform Mg^{2+} and Ni^{2+} ions distribution, and conical nanotube with cation gradient along its side length.

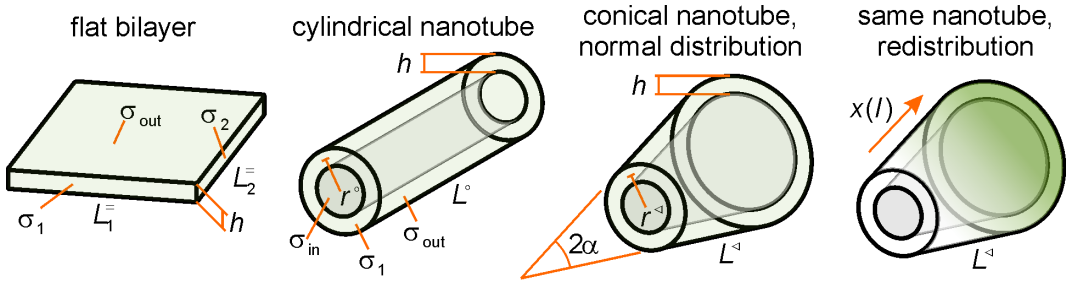

FIG. 2. Four morphological types of hydrosilicate particles and their size parameters. Color gradient denotes Mg^{2+} and Ni^{2+} ions redistribution along the side length of conical nanotube

The energy of each particle type includes strain energy and surface energy components. Before writing these equations, we must specify a number of principle assumptions made. First, processes like the formation of cylindrical and conical nanotubes by scrolling of flat layer, and also cations redistribution do not yield a mass (quantity of substance) change. For the cation redistribution process, the total concentration change must be equal to zero:

$$\frac{\int\limits_0^{L^\triangleleft} dl\,(x(l)-\bar{x})\,[r^\triangleleft/\sin(\alpha)+l]\tan(\alpha)}{\int\limits_0^{L^\triangleleft} dl\,[r^\triangleleft/\sin(\alpha)+l]\tan(\alpha)}=0, \tag{1}$$

where $L^\triangleleft$ is side length of conical nanotube; $x(l)$ is length-dependent local molar content of Ni^{2+} ions; $\bar{x}$ is average molar content of Ni^{2+} ions in respect to sum of Mg and Ni cations; $r^\triangleleft$ is initial (smallest) cone radius of curvature on the half of wall thickness; α is half of cone angle. Integration in denominator returns the cone's surface area.

Second, scrolling process and transformation of flat layer into tube occurs without significant structural and chemical changes, except those mentioned above, and only morphological changes are under consideration here [57]. This also means that bending of the flat layer is small, and we can write strain energy equations in accordance with classic elastic theory [65]. Third, we assume that increase of curvature does not affect structural parameters like the Young's modulus and specific surface energies, although it is imprecise for curvature radii or layer thicknesses less than 3–4 nm [66, 67]. Further assumptions and approximations will be given below.

In analogy with [57], the strain energy of cylindrical nanotube per 1 mol is:

$$E_{\mathrm{s}}^{\circ} = \frac{1}{\nu(\bar{x})}\frac{D_{\mathrm{s}}}{2}2\pi r^{\circ}L^{\circ}\left(\frac{1}{r^{\circ}} - \frac{1}{r_0(\bar{x})}\right)^2 = \frac{Yh^3M(\bar{x})\pi r^{\circ}L^{\circ}}{12\left(1-\mu^2\right)V\rho(\bar{x})}\left(\frac{1}{r^{\circ}} - \frac{1}{r_0(\bar{x})}\right)^2, \tag{2}$$

where $\nu(\bar{x})$ is quantity of substance; D_{s} is bending stiffness; r° is cylinder radius on the half of wall thickness $h/2$; L° is cylinder length; Y is the Young's modulus; μ is the Poisson's ratio; $M(\bar{x})$ is molar mass; V is volume; and $\rho(\bar{x})$ is X-ray (bulk) density. The parameter $r_0(\bar{x})$ is radius of mechanically unstressed bilayer, which depends on cell parameters of octahedral and tetrahedral sublayers, thus, on interatomic distances [59].

Formally, we should denote Y, h, and μ as functions of $\bar{x}$, but the effect of chemical composition is either negligible or too uncertain, especially its influence on the Young's modulus [42]. Pure Mg- and Ni-hydrosilicates can have small difference in the Young's modulus, whereas bending stiffness of Mg- or Ni-doped hydrosilicates (or doped by other elements) is usually higher than that of pure ones [68]. For the rest of the parameters in (2), we assume linear dependence on $\bar{x}$ (i.e. the Vegard's rule is valid). For the flat layer of the same volume and density, the strain energy is:

$$E_{\mathrm{s}}^{=} = \frac{Yh^3M(\bar{x})L_1^{=}L_2^{=}}{24\left(1-\mu^2\right)V\rho(\bar{x})}\frac{1}{r_0^2(\bar{x})} = \frac{Yh^2M(\bar{x})}{24\left(1-\mu^2\right)\rho(\bar{x})r_0^2(\bar{x})}, \tag{3}$$

where $L_1^{=}$ and $L_2^{=}$ are side lengths of the flat layer.

In the case of a conical tube (Fig. 2), calculation of strain energy goes through integration along the side length of the cone:

$$E_{\mathrm{s}}^{\triangleleft} = \frac{D_{\mathrm{s}}}{2\nu(\bar{x})}\int\limits_0^{L^{\triangleleft}} dl\left(\frac{\cot(\alpha)}{[r^{\triangleleft}/\sin(\alpha)+l]} - \frac{1}{r_0(\bar{x})}\right)^2 2\pi\left[r^{\triangleleft}/\sin(\alpha)+l\right]\tan(\alpha). \tag{4}$$

Non-uniform distribution of Mg and Ni cations along the length transforms this equation into:

$$E_{\mathrm{s}}^{\triangleleft\mathrm{g}} = \int\limits_0^{L^{\triangleleft}} dl\frac{D_{\mathrm{s}}}{2\nu(x(l))}\left(\frac{\cot(\alpha)}{[r^{\triangleleft}/\sin(\alpha)+l]} - \frac{1}{r_0(x(l))}\right)^2 2\pi\left[r^{\triangleleft}/\sin(\alpha)+l\right]\tan(\alpha), \tag{5}$$

where r_0 becomes a function of l.

Once again, here we neglect possible dependence of Y, h, and μ on $x(l)$. Furthermore, in current approximation, we do not take into the account the function $\nu(x(l))$ and leave it beyond the integral as $\nu(\bar{x})$. Thus, the additional energy effect caused by special cation distribution might be realized due to minimization of squared difference of curvatures.

Full surface energy of the particles under consideration consists of partial surface energies of each of free surfaces (Fig. 2). For the cylindrical nanotube, it is:

$$\Sigma^{\circ} = \frac{2\pi}{\nu(\bar{x})}\left[\sigma_{\mathrm{out}}\left(r^{\circ}+\frac{h}{2}\right)L^{\circ} + \sigma_{\mathrm{in}}\left(r^{\circ}-\frac{h}{2}\right)L^{\circ} + 2\sigma_1 r^{\circ}h\right], \tag{6}$$

where σ_{out}, σ_{in}, and σ_1 are specific surface energies of outer, inner and cross-section surfaces, accordingly. In current approximation, we consider Mg- and Ni-rich hydrosilicate layers have close values of specific surface energies.

For the flat layer:

$$\Sigma^{=} = \frac{1}{\nu(\bar{x})}\left[L_1^{=}L_2^{=}\left(\sigma_{\mathrm{out}}+\sigma_{\mathrm{in}}\right) + 2\sigma_1 L_1^{=}h + 2\sigma_2 L_2^{=}h\right]. \tag{7}$$

TABLE 1. Structural parameters of the model

Parameter	Mg-chrysotile	Ni-pecoraite	Reference
m g	10^{-16}	10^{-16}	—
$\bar{x}$	0.5	0.5	—
M g/mol	277.1	380.3	—
ρ g/cm^3	2.5	3.5	[59]
r_0 nm	8.8	15	[52, 59]
h nm	0.4	0.4	[69]
t nm	0.3	0.3	[69]
Y GPa	300	300	[42, 51]
μ	0.2	0.2	[70]
σ_{out} J/m^2	0.6	0.6	[71–73]
σ_{in} J/m^2	0.4	0.4	[71–73]
σ_1, σ_2 J/m^2	1.2	1.2	[71–73]

For conical nanotube:

$$\Sigma^{\triangleleft} = \frac{2\pi}{\nu(\bar{x})}\left[\int_0^{L^{\triangleleft}} dl\sigma_{\text{out}}\left(r^{\triangleleft} + l\sin(\alpha) + \frac{h}{2\cos(\alpha)}\right) + \int_0^{L^{\triangleleft}} dl\sigma_{\text{in}}\left(r^{\triangleleft} + l\sin(\alpha) - \frac{h}{2\cos(\alpha)}\right) + \sigma_1 h\left(2r^{\triangleleft} + l\sin(\alpha)\right)\right]. \quad (8)$$

Due to the proximity of specific surface energies of Mg- and Ni-based lattices [59], we neglect changes in surface energy caused by their redistribution, i.e. $\Sigma^{\triangleleft g} \cong \Sigma^{\triangleleft}$. Energy effect of cation redistribution is:

$$\Delta E^{\triangleleft}_{\triangleleft g} = (E_s^{\triangleleft g} + \Sigma^{\triangleleft g}) - (E_s^{\triangleleft} + \Sigma^{\triangleleft})_{\min} \cong E_s^{\triangleleft g} - E^{\triangleleft}_{s,\min}. \quad (9)$$

This equation must be accompanied by constant composition condition (1). We can solve the system of (1) and (9) assuming $x(l)$ is two-parametric, for example, linear function of l:

$$x(l) = a + bl. \quad (10)$$

The choice of linear form of function allows one to not only integrate (5) analytically, but also assign clear physical meaning to the function parameters.

We suggest the following equation procedure: (a) as far as the integration leads to rather complicated forms of equations, we decide to assign numerical values to all structural parameters of energy model and visualize the results without writing analytical solution for energy minima; (b) we determine energy effect of cylindrical nanotube formation with respect to the energy minimum of flat layer:

$$\Delta E^{=}_{\circ} = (E_s^{\circ} + \Sigma^{\circ}) - (E_s^{=} + \Sigma^{=})_{\min}, \quad (11)$$

and find the energy minimum of the tube with the values $r^{\circ}_{\min}$, $L^{\circ}_{\min}$, $E^{\circ}_{s,\min}$, $\Sigma^{\circ}_{\min}$; (c)we put these values in comparison with energy of conical nanotubes without and with linear distribution of the cations.

3. Results and discussion

Table 1 summarizes numerical values of structural parameters that we used in the calculation.

The choice of specific surface energy values becomes a sort of problem. Previous modeling cases (formation of multiwalled cylindrical nanoscrolls [58, 59]) were free from the influence of edges just because their surface areas were assumed to be constant during the scrolling process. Here, we cannot neglect difference in edges surface

areas between cone and cylinder. We chose edge values σ_1 and σ_2 at least 3 times higher the values related to outer and inner surfaces because of higher substance density along these directions.

Figure 3(a) shows the energy effect of cylindrical singlewalled nanotube formation with respect to flat layer (see equation (11)). The energy curve has an asymmetrical minimum with the with the parameters $\Delta E_{\circ}^{=} = -2$ kJ/mol, $r_{\min}^{\circ} = 14.6$ nm, $L_{\min}^{\circ} = 909$ nm. Relative to this point, conical nanotube of any morphology has higher energy (Fig. 3(b)): the larger is the cone angle, the more positive the energy effect is. This result correlates with numerous reports [38–49], in which mostly cylindrical form of chrysotile nanoscrolls and nanotubes has been observed after prolonged hydrothermal treatment. However, the energy effect of conical nanotube, especially when the angle is small ($2\alpha < 5^{\circ}$), does not exceed hundreds of J/mol. This feature also explains why high-angle ($2\alpha > 20^{\circ}$) conical tubes (scrolls) are rarely observed experimentally.

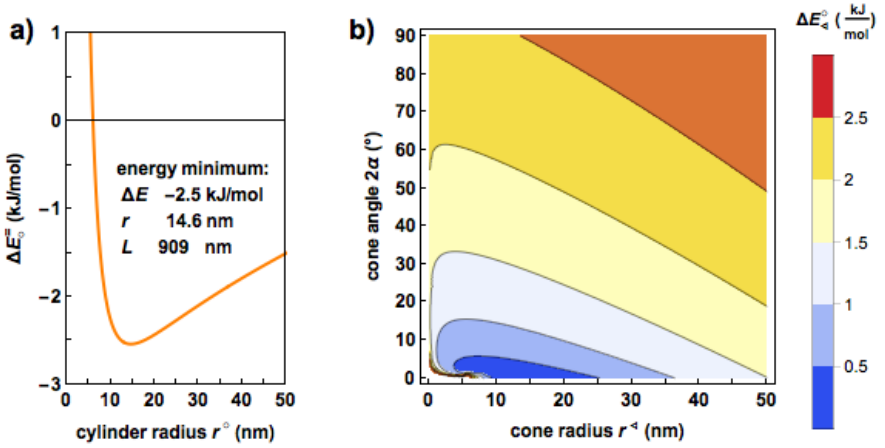

FIG. 3. (a) Energy effect of cylindrical nanotube formation from flat layer versus radius of curvature. (b) Energy effect of conical nanotube formation (with respect to the cylindrical nanotube energy minimum) versus initial radius of curvature and cone angle

Despite being less energetically preferable than the cylinder, the cone of certain angle 2α still has energy minimum (Fig. 3(b)). On the next calculation step, we compared this minimum with the conical nanotube with linear change of Ni^{2+} ion concentration (10).

Figure 4 shows the calculation results for cone angle $2\alpha = 5^{\circ}$. The case of parameter $a < 0.5$ corresponds to "direct" type of distribution (see inset on Fig. 4), in which the cation with bigger ionic radius (Mg^{2+}) concentrates at the small end of the tube, and the cation with smaller ionic radius (Ni^{2+}) – at the big end. $a \cong 0.5$ means absence of cation redistribution, and $a > 0.5$ represents "reverse" cation distribution. The redistribution causes change of energy preferable initial cone radius, which is optimal for certain chemical compositions. The maximal energy effect due to cation redistribution reaches 70–80 J/mol at 2α around 5° (Fig. 5). Interesting that there is a certain cone angle interval, in which the redistribution has maximal impact. If the angle is small, the redistribution does not make substantial contribution. Note there is no need for maximal possible concentration gradient – 0 % Ni at the small end of the nanotube, and 100 % Ni at its large end, i.e. $a = 0$ – in case of small angles ($2\alpha < 2^{\circ}$, Fig. 5(a)). During increase of cone angle the maximal cation gradient becomes less preferable energetically. This is because conical nanotube with large angle tends to increase its initial radius, which becomes unfavorable for only Mg^{2+}-rich hydrosilicate structure.

Choice of linear function $x(l)$ (10) seems to be close to the best way of cations redistribution. To minimize strain energy, according to our approximation, it is sufficient to be:

$$\left(\frac{\cot(\alpha)}{[r^{\triangleleft}/\sin(\alpha) + l]} - \frac{1}{x(l) r_{0,\mathrm{Ni}} + [1 - x(l)]\, r_{0,\mathrm{Mg}}} \right)^2 = 0 \tag{12}$$

Solving this equation regarding $x(l)$ gives:

$$x(l) = \frac{r^{\triangleleft}/\cos(\alpha) - r_{0,\mathrm{Mg}}}{r_{0,\mathrm{Ni}} - r_{0,\mathrm{Mg}}} + l \frac{\tan(\alpha)}{r_{0,\mathrm{Ni}} - r_{0,\mathrm{Mg}}}, \tag{13}$$

which linearly depends on l.

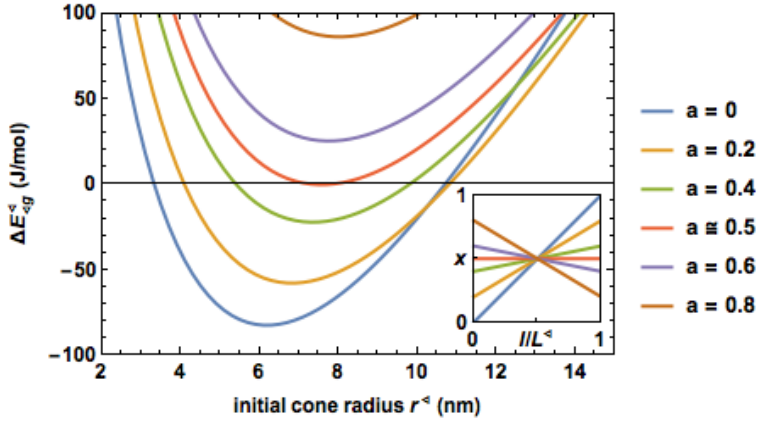

FIG. 4. Energy effect of cations redistribution in conical nanotube with $2\alpha = 5°$. Inset: Ni^{2+} concentration profiles along conical nanotube side length (relative coordinates)

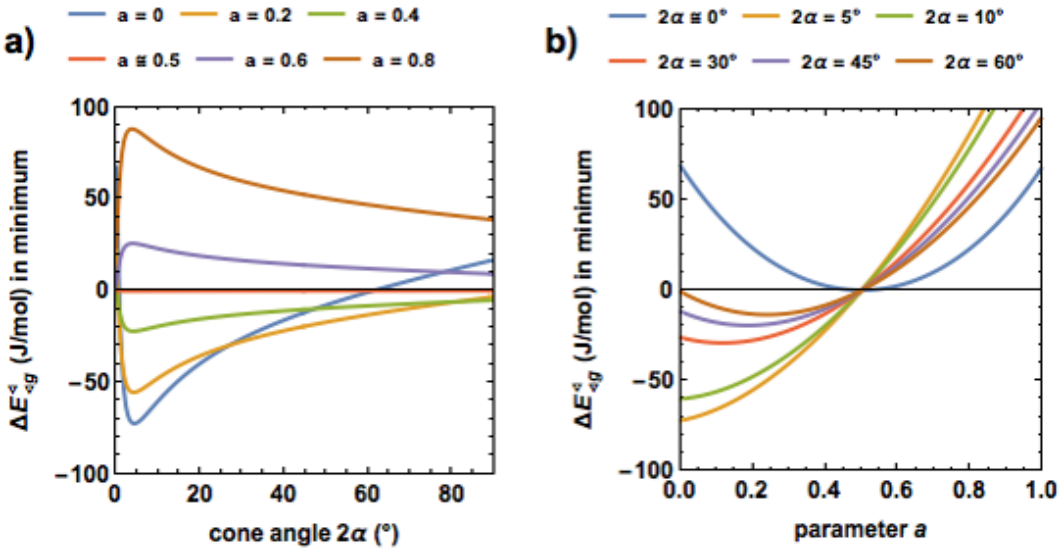

FIG. 5. (a) Depth of energy minimum vs cone angle. (b) Depth of energy minimum vs parameter a

4. Concluding remarks

Here, we developed an energy model for single-walled conical nanotube formation, and redistribution of cations inside its crystal structure as a mechanism to decrease its strain energy. These calculations showed that, in general, conical nanotubes are less energy favorable than the cylindrical nanotubes. At the same time, cation redistribution decreases conical nanotube's energy and make it slightly more preferable in comparison to the tube without redistribution. This additional energy effect, together with sophistication of chemical composition can probably inhibit recrystallization process and thus stabilize conical forms of hydrosilicates during long-time hydrothermal treatments.

Stabilization of conical morphology may occur not only in case of Ni^{2+} doping, but by the addition of other elements, for example, Co and Fe, which have their own preferable radii of curvatures and r_0 values, but among them Ni^{2+} possesses ionic radius closest to Mg^{2+}. This feature allows production of nanotubes in all ranges of Ni^{2+} concentrations, whereas in case of Fe^{3+} doping, there might be some difficulties regarding phase homogeneity.

Conical hydrosilicate nanotubes observed by electron microscopy often have walls consisting of two to tens of layers. Our approach can be extrapolated to those types of objects if we consider them as systems of embedded cones. Finally, cation redistribution may occur either in multi-walled cylindrical nanoscroll or nanotube just because the layers curvature changes from its inner surface to the outer one. The effect of redistribution here may reveal

itself by an increase in the outer diameter (number of layers inside the wall), including formation of cylindrical growth steps on the outer surface of the hydrosilicate nanotube.

Acknowledgements

The research was supported by Russian Science Foundation grant 16-13-10252.

References

[1] Višić B., Panchakarla L.S., Tenne R. Inorganic nanotubes and fullerene-like nanoparticles at the crossroads between solid-state chemistry and nanotechnology. *JACS*, 2017, DOI: 10.1021/jacs.7b01652.
[2] Jana M.K., et al. Two-dimensional inorganic analogues of graphene: transition metal dichalcogenides. *Philos. Trans. A*, 2016, **374** (2076), P. 162–163.
[3] Tenne R., Seifert G. Recent progress in the study of inorganic nanotubes and fullerene-like structures. *Annu. Rev. Mater. Res.*, 2009, **39** (1), P. 387–413.
[4] Tagliazucchi M., Szleifer I. Salt pumping by voltage-gated nanochannels. *J. Phys. Chem. Lett.*, 2015, **6** (18), P. 3534–3539.
[5] Huang J.Y., et al. Nanowire liquid pumps. *Nat. Nanotechnol.*, 2013, **8** (4), P. 277–281.
[6] Iijima S. Helical microtubules of graphitic carbon. *Nature*, 1991, **354** (6348), P. 56–58.
[7] Enyashin A.N., Ivanovskii A.L. Electronic structure of nanotubes of layered modifications of carbon nitride C_3N_4. *Dokl. Phys. Chem.*, 2004, **398** (1–3), P. 211–215.
[8] Tenne R., et al. Polyhedral and cylindrical structures of tungsten disulphide. *Nature*, 1992, **360** (6403), P. 444–446.
[9] Prinz V.Y., et al. Free-standing and overgrown InGaAs/GaAs nanotubes, nanohelices and their arrays. *Physica E*, 2000, **6** (1–4), P. 828–831.
[10] Prinz V.Y. A new concept in fabricating building blocks for nanoelectronic and nanomechanic devices. *Microelectron. Eng.*, 2003, **69** (2–4), P. 466–475.
[11] Gurenko V.E., Tolstoy V.P., Gulina L.B. The effect of microtube formation with walls, containing Fe_3O_4 nanoparticles, via gassolution interface technique by hydrolysis of the $FeCl_2$ and $FeCl_3$ mixed solution with gaseous ammonia. *Nanosyst.: Phys. Chem. Math.*, 2017, **8** (4), P. 471–475.
[12] Gulina L.B., et al. Facile synthesis of LaF_3 strained 2D nanoparticles and microtubes at solution–gas interface. *J. Fluor. Chem.*, 2015, **180**, P. 117–121.
[13] Poluektov P.P., Dmitriev M.S. Model of nanotube formation in solution under molecular sorption conditions. *At. Energy*, 2009, **106** (5), P. 343–347.
[14] Enyashin A.N., Ivanovskii A.L. Theoretical prediction of $Al(OH)_3$ nanotubes and their properties. *Physica E*, 2008, **41** (2), P. 320–323.
[15] Grigor'eva A.V., et al. Micromorphology and structure of vanadium oxide nanotubes. *Dokl. Chem.*, 2006, **410** (2), P. 165–169.
[16] Korytkova E.N., Pivovarova L.N. Hydrothermal synthesis of nanotubes based on $(Mg,Fe,Co,Ni)_3Si_2O_5(OH)_4$ hydrosilicates. *Glas. Phys. Chem.*, 2010, **36** (1), P. 53–60.
[17] Vahedi V., Pasbakhsh P., Chai S.P. Toward high performance epoxy/halloysite nanocomposites: New insights based on rheological, curing, and impact properties. *Mater. Des.*, 2015, **68**, P. 42–53.
[18] Yudin V.E., et al. Effects of nanofiller morphology and aspect ratio on the rheo-mechanical properties of polyimide nanocomposites. *Express Polym. Lett.*, 2008, **2** (7), P. 485–493.
[19] Afanas'eva N.V., et al. Relaxation processes in an aromatic polyamide-imide and composites on its basis with hydrosilicate nanoparticles. *Polym. Sci. Ser. A*, 2016, **58** (6), P. 956–967.
[20] Naffakh M., et al. New hybrid nanocomposites containing carbon nanotubes, inorganic fullerene-like WS2 nanoparticles and poly(ether ether ketone) (PEEK). *J. Mater. Chem.*, 2011, **21** (20), P. 7425–7433.
[21] Ksenevich V.K., et al. Electrical properties of carbon nanotubes/WS2 nanotubes (nanoparticles) hybrid films. *Nanosyst.: Phys. Chem. Math.*, 2016, **7** (1), P. 37–43.
[22] Lvov Y., et al. Halloysite clay nanotubes for loading and sustained release of functional compounds. *Adv. Mater.*, 2016, **28** (6), P. 1227–1250.
[23] Cheng L., et al. Removal of simulated radionuclide Ce(III) from aqueous solution by as-synthesized chrysotile nanotubes. *Chem. Eng. J.*, 2012, **213**, P. 22–30.
[24] Zheng Y., et al. Poly(methacrylic acid)-graft-$Ni_3Si_2O_5(OH)_4$ multiwalled nanotubes as a novel nanosorbent for effective removal of copper(II) ions. *Colloids Surfaces A*, 2016, **502**, P. 89–101.
[25] Zhang Y., et al. Substitutional doping for aluminosilicate mineral and superior water splitting performance. *Nanoscale Res. Lett.*, 2017, **12** (1), P. 456.
[26] Sarvaramini A., Larachi F. Mössbauer spectroscopy and catalytic reaction studies of shrysotile-catalyzed steam reforming of benzene. *J. Phys. Chem. C*, 2011, **115** (14), P. 6841–6848.
[27] Bian Z., et al. A highly active and stable Ni–Mg phyllosilicate nanotubular catalyst for ultrahigh temperature water-gas shift reaction. *Chem. Commun.*, 2015, **51** (91), P. 16324–16326.
[28] Peng H., et al. Facile synthesis and characterization of core-shell structured Ag_3PO_4@Hal nanocomposites for enhanced photocatalytic properties. *Appl. Clay Sci.*, 2017, **141**, P. 132–137.
[29] Yang Y., et al. $Ni_3Si_2O_5(OH)_4$ multi-walled nanotubes with tunable magnetic properties and their application as anode materials for lithium batteries. *Nano Res.*, 2011, **4** (9), P. 882–890.
[30] Shafia E., et al. Isomorphic substitution of aluminium by iron into single-walled alumino-silicate nanotubes: A physico-chemical insight into the structural and adsorption properties of Fe-doped imogolite. *Microp. Mesop. Mater.*, 2016, **224**, P. 229–238.
[31] Lafay R., et al. Influence of trace elements on the textural properties of synthetic chrysotile: Complementary insights from macroscopic and nanoscopic measurements. *Microp. Mesop. Mater.*, 2014, **183**, P. 81–90.
[32] Yuan P., Tan D., Annabi-Bergaya F. Properties and applications of halloysite nanotubes: recent research advances and future prospects. *Appl. Clay Sci.*, 2015, **112-113**, P. 75–93.

[33] Pollastri S., et al. The crystal structure of mineral fibres: 1. Chrysotile. *Period. di Mineral.*, 2016, **85** (3), P. 249–259.
[34] Villanova-de-Benavent C., et al. Ni-phyllosilicates (garnierites) from the Falcondo Ni-laterite deposit (Dominican Republic): Mineralogy, nanotextures, and formation mechanisms by HRTEM and AEM. *Am. Mineral.*, 2016, **101** (6), P. 1460–1473.
[35] Krasilin A.A., et al. Formation of conical $(Mg,Ni)_3Si_2O_5(OH)_4$ nanoscrolls. *Dokl. Phys. Chem.*, 2015, **460** (2), P. 42–44.
[36] Momma K., Izumi F. VESTA 3 for three-dimensional visualization of crystal, volumetric and morphology data. *J. Appl. Crystallogr.*, 2011, **44** (6), P. 1272–1276.
[37] Falini G., et al. Tubular-shaped stoichiometric chrysotile nanocrystals. *Chem. Eur. J.*, 2004, **10** (12), P. 3043–3049.
[38] Korytkova E.N., et al. Formation of $Mg_3Si_2O_5(OH)_4$ Nanotubes under hydrothermal conditions. *Glas. Phys. Chem.*, 2004, **30** (1), P. 51–55.
[39] Jancar B., Suvorov D. The influence of hydrothermal-reaction parameters on the formation of chrysotile nanotubes. *Nanotechnology*, 2006, **17** (1), P. 25–29.
[40] Krasilin A.A., Almjasheva O.V., Gusarov V.V. Effect of the structure of precursors on the formation of nanotubular magnesium hydrosilicate. *Inorg. Mater.*, 2011, **47** (10), P. 1111–1115.
[41] Lafay R., et al. Dissolution-reprecipitation and self-assembly of serpentine nanoparticles preceding chrysotile formation: Insights into the structure of proto-serpentine. *Am. Mineral.*, 2016, **101** (12), P. 2666–2676.
[42] Piperno S., et al. Characterization of geoinspired and synthetic chrysotile nanotubes by atomic force microscopy and transmission electron microscopy. *Adv. Funct. Mater.*, 2007, **17** (16), P. 3332–3338.
[43] Bloise A., et al. Synthesis of Fe-doped chrysotile and characterization of the resulting chrysotile fibers. *Cryst. Res. Technol.*, 2009, **44** (6), P. 590–596.
[44] Korytkova E.N., et al. Hydrothermal synthesis of nanotubular Co-Mg hydrosilicates with the chrysotile structure. *Russ. J. Gen. Chem.*, 2007, **77** (10), P. 1669–1676.
[45] Bloise A., et al. Influence of synthesis conditions on growth of Ni-doped chrysotile. *Microp. Mesop. Mater.*, 2010, **132** (1-2), P. 239–245.
[46] McDonald A., Scott B., Villemure G. Hydrothermal preparation of nanotubular particles of a 1:1 nickel phyllosilicate. *Microp. Mesop. Mater.*, 2009, **120** (3), P. 263–266.
[47] Korytkova E.N., et al. Synthesis of nanotubular $Mg_3Si_2O_5(OH)_4$–$Ni_3Si_2O_5(OH)_4$ silicates at elevated temperatures and pressures. *Inorg. Mater.*, 2005, **41** (7), P. 743–749.
[48] Krasilin A.A., et al. Morphology vs. chemical composition of single Ni-doped hydrosilicate nanoscroll. *Mater. Lett.*, 2016, **171**, P. 68–71.
[49] White R.D., Bavykin D.V., Walsh F.C. Morphological control of synthetic $Ni_3Si_2O_5(OH)_4$ nanotubes in an alkaline hydrothermal environment. *J. Mater. Chem. A*, 2013, **1** (3), P. 548–556.
[50] Guimarães L., et al. Structural, electronic, and mechanical properties of single-walled halloysite nanotube models. *J. Phys. Chem. C*, 2010, **114** (26), P. 11358–11363.
[51] Loureno M.P., et al. Structural, electronic, and mechanical properties of single-walled chrysotile nanotube models. *J. Phys. Chem. C*, 2012, **116** (17), P. 9405–9411.
[52] Demichelis R., et al. Serpentine polymorphism: a quantitative insight from first-principles calculations. *Cryst. Eng. Comm.*, 2016, **18** (23), P. 4412–4419.
[53] Singh B. Why does halloysite roll? – A new model. *Clays Clay Miner.*, 1996, **44** (2), P. 191–196.
[54] Chivilikhin S.A., Popov I.Yu., Gusarov V.V. Dynamics of nanotube twisting in a viscous fluid. *Doklady Physics*, 2007, **52** (1), P. 60–62.
[55] Thill A., et al. How the diameter and structure of $(OH)_3Al_2O_3Si_xGe_{1x}OH$ imogolite nanotubes are controlled by an adhesion versus curvature competition. *J. Phys. Chem. C*, 2012, **116** (51), P.26841–26849.
[56] Thill A., Picot P., Belloni L. A mechanism for the sphere/tube shape transition of nanoparticles with an imogolite local structure (imogolite and allophane). *Appl. Clay Sci.*, 2017, **141**, P. 308–315.
[57] Krasilin A.A., Gusarov V.V. Energy of formation of chrysotile nanotubes. *Russ. J. Gen. Chem.*, 2014, **84** (12), P. 2359–2363.
[58] Krasilin A.A., Gusarov V.V. Energy model of radial growth of a nanotubular crystal. *Tech. Phys. Lett.*, 2016, **42** (1), P. 55–58.
[59] Krasilin A.A., Nevedomsky V.N., Gusarov V.V. Comparative energy modeling of multiwalled $Mg_3Si_2O_5(OH)_4$ and $Ni_3Si_2O_5(OH)_4$ nanoscroll growth. *J. Phys. Chem. C*, 2017, **121** (22), P. 12495–12502.
[60] Foresti E., et al. Morphological and chemical/physical characterization of Fe-doped synthetic chrysotile nanotubes. *Adv. Funct. Mater.*, 2005, **15** (6), P. 1009–1016.
[61] Korytkova E.N., et al. Hydrothermal synthesis of nanotubular Mg–Fe hydrosilicate. *Russ. J. Inorg. Chem.*, 2007, **52** (3), P. 338–344.
[62] Krasilin A.A., Gusarov V.V. Control over morphology of magnesium-aluminum hydrosilicate nanoscrolls. *Russ. J. Appl. Chem.*, 2015, **88** (12), P. 1928–1935.
[63] Krasilin A.A., et al. Formation of variable-composition iron(III) hydrosilicates with the hrysotile structure. *Russ. J. Gen. Chem.*, 2016, **86** (12), P. 2581–2588.
[64] Smolikov A., et al. Morphology of synthetic chrysotile nanofibers (Mg-hydro silicate). *J. Mater. Sci. Eng. A*, 2013, **3** (8), P. 523–530.
[65] Landau L.D., et al. *Theory of elasticity*, third edition: Volume 7 (course of theoretical physics). Butterworth-Heinemann, Oxford, 1986, 187 p.
[66] Tolman R.C. The effect of droplet size on surface tension. *J. Chem. Phys.*, 1949, **17** (3), P. 333.
[67] Krivtsov A.M., Morozov N.F. On mechanical characteristics of nanocrystals. *Phys. Solid State*, 2002, **44** (12), P. 2260–2265.
[68] Krasilin A.A., et al. Interconnection between composition, morphology and mechanics of chrysotile nanoscroll. *Proceedings of the Conference "12th Multinational Congress on Microscopy MCM 2015"*, Eger, Hungary, August 23–28, 2015, P. 459–460.
[69] Roveri N., et al. Geoinspired synthetic chrysotile nanotubes. *J. Mater. Res.*, 2006, **21** (11), P. 2711–2725.
[70] Cressey B.A., Whittaker E.J.W. Five-fold symmetry in chrysotile asbestos revealed by transmission electron microscopy. *Mineral. Mag.*, 1993, **57** (389), P. 729–732.
[71] Tasker P.W., Duffy D.M. The structure and properties of the stepped surfaces of MgO and NiO. *Surf. Sci.*, 1984, **137** (1), P. 91–102.
[72] Evarestov R.A., Bandura A.V. HF and DFT calculations of MgO surface energy and electrostatic potential using two- and three-periodic models. *Int. J. Quantum Chem.*, 2004, **100** (4), P. 452–459.
[73] Shchipalov Y.K. Surface energy of crystalline and vitreous Silica. *Glas. Ceram.*, 2000, **57** (11/12), P. 374–377.